

## Chapter 2

# Physical and Optical properties of aerosols

### 2.1 Size distributions

As the sizes of aerosols span over a wide range of magnitudes, from about  $0.001 \mu\text{m}$  to  $100 \mu\text{m}$  an individual description of aerosols becomes an arduous task. The spread in the sizes of aerosols is due to intricate processes that create the particles, the interactions among themselves and processes that remove these particles from the atmosphere. The spread of the aerosol particle population over the vast size range is described by a *size distribution function*, in which the sizes of particles are represented by their radii. Essentially a size distribution function describes the number of particles per specified interval of radius. Size distribution is perhaps the basic aerosol parameter used in determining other properties of aerosols, provided their composition and physical state are known. Though many size distribution representations are possible, the discretion of opting for a harmonious size distribution function rests mainly on the considerations of the property to be emphasised apart from the preference of the researcher, limited by measurement techniques. There exist atleast three major size distributions for characterising atmospheric aerosols, namely,

- (1) Junge power law size distribution
- (2) Lognormal size distribution and
- (3) Modified Gamma distribution.

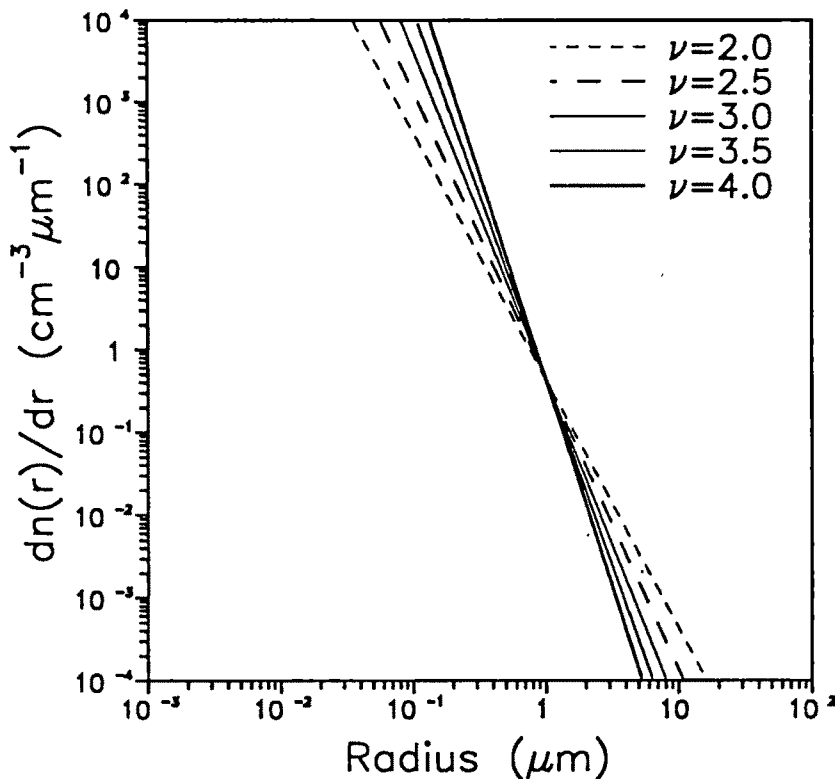


Figure 2.1: Aerosol size distributions obeying Junge power law for exponents  $\nu$ , varying from 2 to 4.

### 2.1.1 Junge power law size distribution

Junge was among the first scientists to have recognised the need for using logarithmic scales for the illustration of size distributions. Junge [1958] based on experimental observations, proposed a power law size distribution function of the form

$$\frac{dn(r)}{d(\log r)} = cr^{-\nu} \quad (2.1)$$

where  $dn(r)$  represents the number of particles with radii between  $r$  and  $r+dr$ ,  $c$  is a constant, depending on the number of particles in one cubic centimetre and the exponent  $\nu$ , determines the slope of the curve (Figure 2.1). As  $\nu$  value decreases the number of larger particles increases compared to the number of smaller particles. For typical

hazes  $\nu$  takes a value of about 3 and fogs are characterised by  $\nu = 2$ . The smallest aerosol particles are the molecular complexes of the small and intermediate ions. These, however do not play an important role in light scattering because of their small size and relatively low concentrations. The size range of interest however starts from  $0.04 \mu\text{m}$  where normally the bulk of the aerosol particles is found. From this radius up to  $10 \mu\text{m}$  the aerosol size distribution more or less follows a power law. The physical explanation of the lower boundary radius is that according to Smoluchowsky's theory, a greater coagulation rate is caused due to increasing number of particles and consequently the small particles coagulate more quickly than the larger ones so that within half a day, the number of particles of the size  $0.01 \mu\text{m}$  is reduced to a negligible amount and hence the number of larger particles is increased. The upper boundary radius ( $10 \mu\text{m}$ ) falls in the range of giant nuclei and particles of larger size are more effectively removed mainly through sedimentation and rainwash [Bullrich, 1964]. The advantage of this size distribution resides in the possibility of describing a size distribution from the knowledge of  $\nu$  only.

Though it's claimed that this law does not explain or accommodate the smaller particle range as well as the larger particle range adequately, in a given volume of aerosol the number of large particles is orders of magnitude less compared to that of small particles and hence particles of size  $10 \mu\text{m}$  and above have relatively insignificant contribution to the total scattered intensity or to the extinction. Similarly in the lower size range even though the number densities are large, the scattering efficiency is much less and they tend to behave more like air molecules. It is found that in the 'optically effective' particle size range of  $0.05 \mu\text{m}$  to  $10 \mu\text{m}$ , Junge power law can be taken as a good representation of aerosol size distribution as the Mie scattering contribution of the smaller particles (less than about  $0.05 \mu\text{m}$ ) to the total integrated intensity is marginal. It has also been found that the total aerosol extinction coefficient is found to increase by 0.4% or less if the power law is truncated at  $r_{\min}$  of  $0.01 \mu\text{m}$  instead of  $0.05 \mu\text{m}$  [Ramachandran et al., 1994c].

### 2.1.2 Lognormal distribution

The lognormal distribution [Davies, 1974] developed on the basis of the distribution of particles originating from a single source through a single production mechanism can be written as

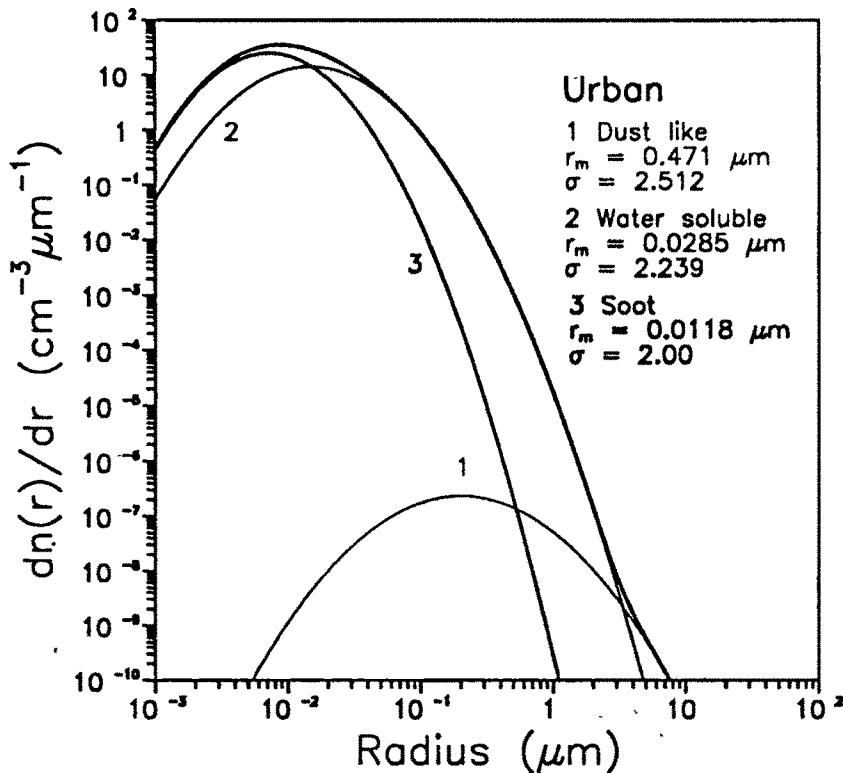


Figure 2.2: A typical lognormal aerosol size distribution for an urban aerosol model which encompasses three different modes, representative of three individual sources. The values are taken from d'Almeida et al. [1991].

$$\frac{dn(r)}{dr} = \frac{A}{\sqrt{2\pi} \ln \sigma} \frac{1}{r} \exp \left[ -\frac{\ln^2 \left( \frac{r}{r_m} \right)}{2 (\ln \sigma)^2} \right] \quad (2.2)$$

where  $A$  is the total number concentration ( $\text{cm}^{-3}$ ),  $\sigma$  is the width of the lognormal curve and  $r_m$  is the mode radius. For a mixture of particles originating from multiple independent sources, the resulting size distribution is a combination of all individual sources.

The lognormal distribution (LND) function lays emphasis on the individual components in a mixture of particles originating from different sources. Each component has its specific mode radius and standard deviation ( $\sigma$ ) and its assigned refractive index. For example the size distribution of an urban aerosol model which is made up of dust like, water soluble and soot components is plotted in Figure 2.2.

The geographical importance of each component depends on the distance from its

source of production as well as its ability to remain airborne and travel long distances [d'Almeida *et al.*, 1991]. For these reasons, it becomes clear that lognormal distributions are best suited to characterise the aerosol components, the aerosol types and their spatial and temporal variability and hence it is widely used for tropospheric studies.

While in the Junge power law distribution  $\nu$  alone is sufficient to describe the aerosol characteristics, in the lognormal distribution the width of the size distribution  $\sigma$  and mode radius  $r_m$  are vital.

A simplified version of the lognormal distribution is zero order logarithmic distribution (ZOLD). This size distribution is used normally after a major volcanic eruption, when the aerosol particles are nonsoluble and is written as

$$\frac{dn(r)}{dr} = A \exp \left[ -\frac{\ln^2 \left( \frac{r}{r_m} \right)}{2(\ln \sigma)^2} \right] \quad (2.3)$$

where A is an arbitrary constant and  $\sigma = 1.8$  [Pinnick *et al.*, 1976].

It is a property of the ZOLD that a change in the mode radius  $r_m$  does not affect the width of the distribution or in other words for all  $\sigma$ s the  $r_m$  value will not change as the radius of maximum concentration or the geometric mean radius  $r_g = r_m$  in the case of ZOLD, while in LND  $r_g = r_m \exp [-(\ln \sigma)^2]$  (Figures 2.3a and 2.3b).

### 2.1.3 Modified Gamma distribution

The modified Gamma distribution was originally proposed for clouds. In its general form the function may be written as

$$\frac{dn(r)}{dr} = A r^\alpha \exp(-b r^\gamma) \quad (2.4)$$

representing a family of size distributions with A,  $\alpha$ , b and  $\gamma$  positive constants which depend on each other. The integration of the above equation over the entire radius range yields the total number of particles per unit volume. The function owes its name to the presence of  $\gamma$ . In the original Gamma distribution  $\gamma = 1$ .

*Deirmendjian* [1964] used this function and computed scattering and polarisation properties of clouds and hazes in the visible as well as in the infrared and he observed that the results compared fairly well with measurements both on natural water clouds and aerosols. The mode radius  $r_m$  was obtained by setting the derivative of the equation to

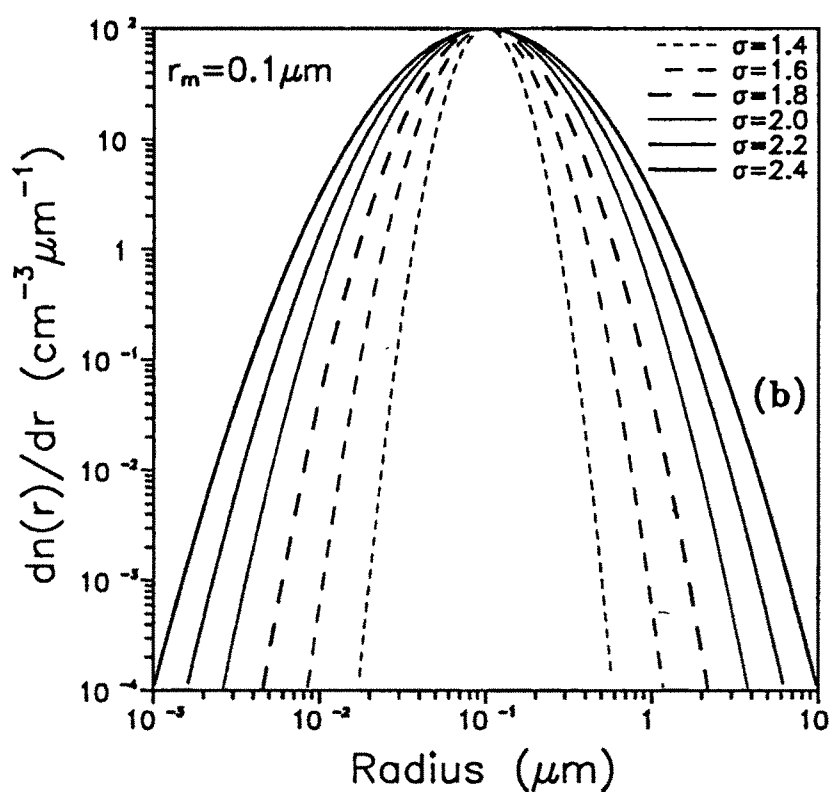
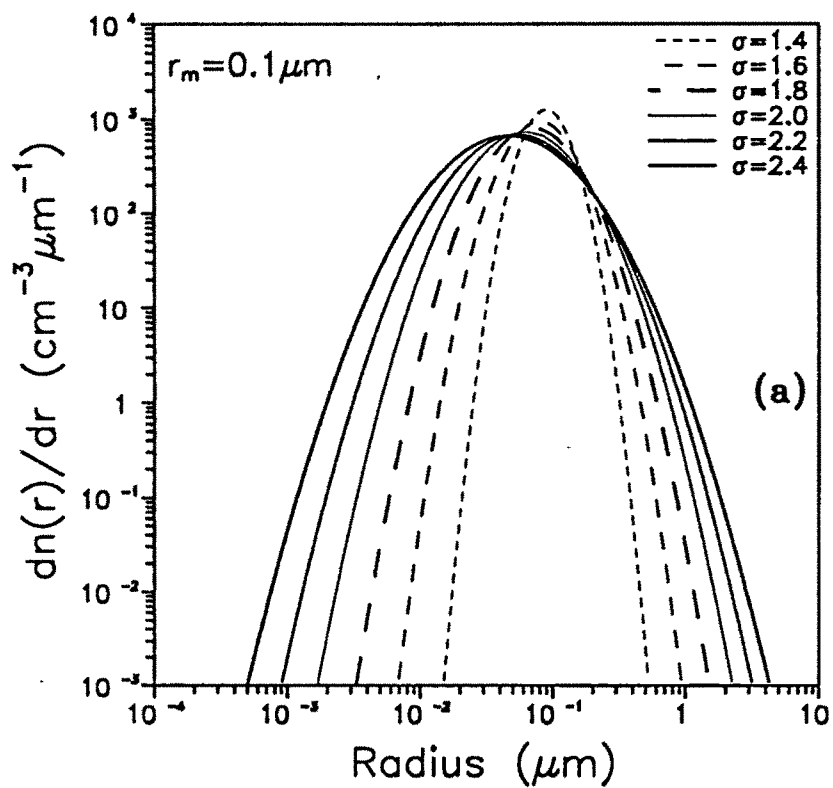


Figure 2.3: Lognormal (top) and zero order logarithmic (bottom) distributions for a mode radius of  $0.1 \mu\text{m}$  and for various widths of size distributions  $\sigma$ , from 1.4 to 2.4.

0. The modified Gamma distribution has great adaptability and can be fitted to various models of haze, cloud and rain, as it contains four adjustable parameters. However, while the slope  $\nu$  in the Junge power law is often correlated with the Ångström's wavelength exponent  $\alpha$  as  $\nu = \alpha + 2$ , which essentially specifies the behaviour of the aerosol extinction and hence the atmospheric turbidity, both Gamma and modified Gamma distribution functions are not very popular, as there is no definitive correlation with aerosol extinction and also the physical meaning of the parameters  $A$ ,  $\alpha$ ,  $b$  and  $\gamma$  is not well understood. Above all, the flexibility of adjusting four parameters, itself turns out to be a drawback as it makes these distributions difficult to handle.

## 2.2 Optical properties

### 2.2.1 Scattering processes

*Scattering* is the process by which a particle in the path of an electromagnetic wave continuously extracts energy from the incident wave and reradiates that energy in all the  $4\pi$  directions.

Scattering can be broadly classified into two categories (i) the elastic scattering, in which the wavelength of the scattered radiation is same as the incident radiation and (ii) inelastic scattering, in which the wavelength of the scattered radiation is different from that of the incident radiation. The elastic scattering can further be classified into two, *Rayleigh scattering* and *Mie scattering* depending on the size of the particle as compared to the wavelength of the incident radiation. When the particle radius is much smaller than the incident wavelength ( $< 0.03\lambda$ ,  $\lambda$  being the wavelength), the scattering is called Rayleigh scattering, named after the scientist who first developed the theory of scattering by very small isotropic particles. Air molecules are the chief Rayleigh scatterers in the atmosphere. Rayleigh scattering varies inversely as the fourth power of the wavelength, with equal amount of fluxes scattered in both forward and backward hemispheres.

Scattering is explained in terms of the electromagnetic theory. The electric field of the incident wave sets in oscillation of electric charges in the particle. When the particle is smaller than the wavelength of the incident radiation, as in the case of Rayleigh scattering, an electric dipole is set up and the scattering is symmetric as an electric dipole radiates

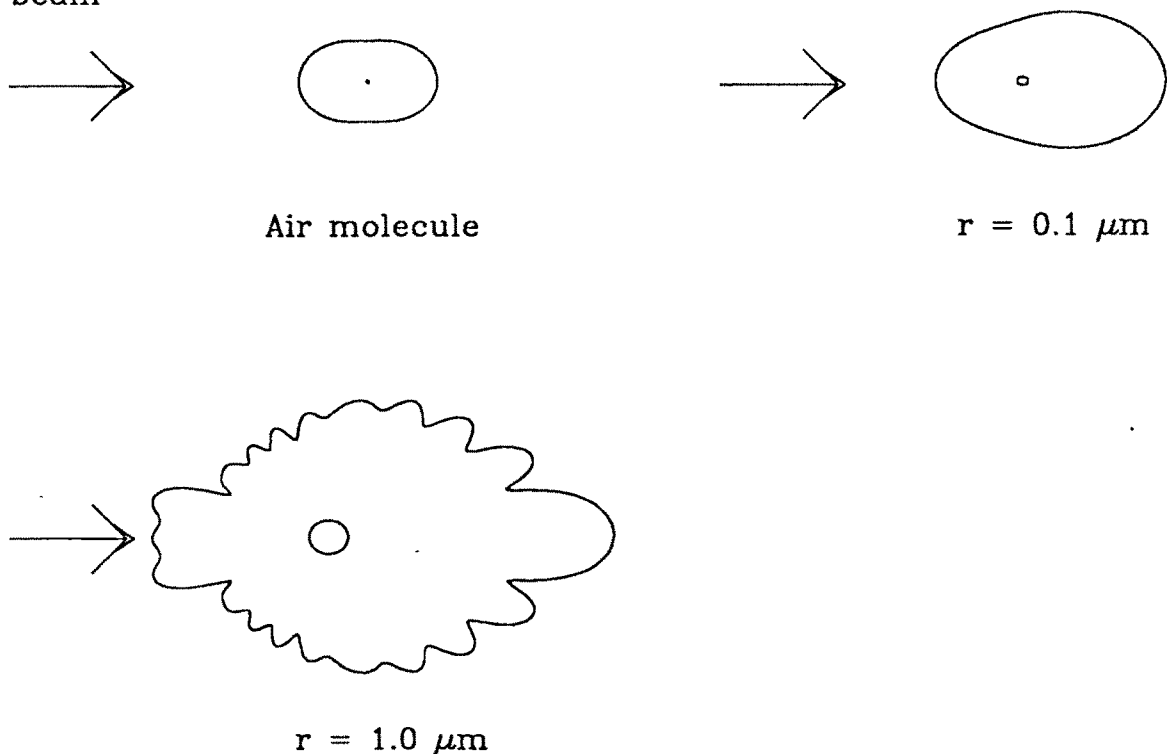


Figure 2.4: *Schematic diagrams of the angular distribution of the scattered radiation intensities for particles of different sizes at  $\lambda = 0.55 \mu\text{m}$ .*

equal amount of fluxes in both forward and backward directions (Figure 2.4).

As the particle dimensions become appreciable to the incident wavelength the scattering process can no longer be explained by merely an induced dipole, a three dimensional charge distribution is set up within the particle with higher moments like quadrupole, octupole, hexadecapole etc. and the scattering process becomes complex. The exact solution to the scattering problem was given by Gustav Mie in 1908 in terms of Maxwell equations and encompasses Rayleigh scattering as a special case. The most notable feature in Mie scattering is the development of forward peak. As the particle size increases the scattering is no more symmetric and more and more radiation is scattered in the forward direction than in the backward direction (Figure 2.4).

### 2.2.2 Mie scattering

If  $i_1$  and  $i_2$  are the polarised components of the scattered intensity resolved perpendicular and parallel to the plane of scattering, then

$$i_1(\alpha, m, \theta) = |S_1|^2 = \left| \sum_{n=1}^{\infty} \frac{2n+1}{n(n+1)} (a_n \pi_n(\cos\theta) + b_n \tau_n(\cos\theta)) \right|^2 \quad (2.5)$$

$$i_2(\alpha, m, \theta) = |S_2|^2 = \left| \sum_{n=1}^{\infty} \frac{2n+1}{n(n+1)} (b_n \pi_n(\cos\theta) + a_n \tau_n(\cos\theta)) \right|^2 \quad (2.6)$$

where  $S_1$  and  $S_2$  are the amplitudes of the scattered radiations  $i_1$  and  $i_2$ . The complex numbers  $a_n$  and  $b_n$  are the Mie coefficients. The functions  $\pi_n$  and  $\tau_n$  depend only on the scattering angle  $\theta$ , the derivatives of Legendre polynomials having an order  $n$  and argument  $\cos\theta$ .  $\alpha$  is the size parameter  $2\pi r/\lambda$  where  $\lambda$  is the wavelength of the incident radiation.

Mie coefficients  $a_n$  and  $b_n$  determine the optical properties such as efficiency factors for extinction ( $Q_{\text{ext}}$ ), scattering ( $Q_{\text{sca}}$ ) and absorption ( $Q_{\text{abs}}$ ).

$$Q_{\text{ext}} = \left(\frac{2}{\alpha^2}\right) \sum_{n=1}^{\infty} (2n+1) \text{Re}(a_n + b_n) \quad (2.7)$$

$$Q_{\text{sca}} = \left(\frac{2}{\alpha^2}\right) \sum_{n=1}^{\infty} (2n+1) (|a_n|^2 + |b_n|^2) \quad (2.8)$$

$$Q_{\text{abs}} = Q_{\text{ext}} - Q_{\text{sca}} \quad (2.9)$$

The extinction coefficient  $\beta_{\text{ext}}$  indicates the fraction of energy removed, per unit path length, from an incident wave with energy flux density 1 by a collection of aerosol particles characterised by the particle size distribution. The energy that then reappears as the scattered energy is the scattering coefficient  $\beta_{\text{sca}}$  and the energy absorbed produces the absorption coefficient  $\beta_{\text{abs}}$ . The sum of scattering and absorption yields the extinction.

$$\beta_{\text{ext,sca,abs}}(\lambda) = \int_{r_1}^{r_2} \frac{dn(r)}{dr} Q_{\text{ext,sca,abs}}(m, \lambda, r) \pi r^2 dr \quad (2.10)$$

where  $dn(r)/dr$  is the number of particles per  $\text{cm}^3$  whose radii are between  $r$  and  $r+dr$ ,  $Q_{\text{ext,sca,abs}}(m, \lambda, r)$  is the Mie extinction /scattering/absorption efficiency factor and  $m$  is the refractive index of aerosol particle.

The single scattering albedo  $\omega_0$  is defined as the fraction of energy removed from the incident beam which reappears as scattered radiation.  $\omega_0$  is equal to 0 for a perfectly absorbing aerosol and is 1 for a pure scatterer and is written as,

$$\omega_0(\lambda) = \frac{\beta_{\text{sca}}(\lambda)}{\beta_{\text{ext}}(\lambda)} = 1 - \frac{\beta_{\text{abs}}(\lambda)}{\beta_{\text{ext}}(\lambda)} \quad (2.11)$$

The aerosol scattering phase function  $P_a(\lambda, \theta)$  is computed using Mie algorithm as

$$P_a(\lambda, \theta) = \frac{\lambda}{(2\pi)^2} \int_{r_1}^{r_2} i(r, \theta) \frac{dn(r)}{dr} dr \quad (2.12)$$

and normalised to unity such that

$$2\pi \int_0^\pi P_a(\lambda, \theta) \sin\theta d\theta = 1. \quad (2.13)$$

The phase function represents the angular distribution of the scattered energy i.e. the angular dependence of scattering. The 'normalised phase function' describes what fraction of scattered radiation appears per unit solid angle in the direction  $\theta$ .

The asymmetry factor  $g$  is defined as the average of the cosine of the scattering angles for scattered radiation such that,

$$g = \frac{\int_0^\pi \cos\theta P_a(\lambda, \theta) d(\cos\theta)}{\int_0^\pi P_a(\lambda, \theta) d(\cos\theta)} \quad (2.14)$$

Theoretically,  $g$  can vary between  $-1$  and  $+1$ . For particles with isotropic scattering properties  $g = 0$ . When scattering is entirely in the forward direction asymmetry factor equals one. The more the particles scatter in the forward direction, which is the case with larger particles the higher is the asymmetry factor.

The integration of extinction coefficient over a path length through the atmosphere yields the optical depth,  $\tau$ .

### 2.2.3 Mie scattering of individual particle

#### Variation of Mie scattering parameters with size of the particle

By and large, the refractive indices of atmospheric particles and molecules are constituted of a real part  $m_r$  and an imaginary part  $m_i$  corresponding, respectively to the scattering and absorption properties. In the solar visible spectrum, as the imaginary parts of the refractive indices of air molecules are insignificantly small, they can be neglected in the scattering discussion.

The behaviour of  $Q_{\text{ext}}$ ,  $Q_{\text{sca}}$  and  $Q_{\text{abs}}$  for single particle of various sizes and various types of aerosols, with varied imaginary refractive indices and their implications will be discussed here. Figures 2.5a-d show the behaviour of  $Q_{\text{ext}}$ ,  $Q_{\text{sca}}$  and  $Q_{\text{abs}}$  for different aerosol types. All these calculations are done for  $\lambda = 550$  nm. The real and imaginary parts of the refractive index are specified in the diagrams. As soot has an imaginary refractive index of 0.44 at 550 nm, the extinction is only due to absorption till about  $0.06 \mu\text{m}$  and the scattering contribution is orders of magnitude less and the curves are very smooth, throughout the radius range. In dust like particle, though initially the contribution comes from only absorption till  $0.02 \mu\text{m}$ , beyond this radius, scattering contributes most to the extinction. In stark contrast, in both 75%  $\text{H}_2\text{SO}_4$  and oceanic type particles, the extinction is only due to scattering throughout from  $0.001 \mu\text{m}$  to  $10 \mu\text{m}$ , while the absorption is orders of magnitude less, as they have very low imaginary refractive indices. In 75%  $\text{H}_2\text{SO}_4$  and oceanic, the curves of extinction and scattering, which are one and the same, tend to oscillate from about  $0.2 \mu\text{m}$  about a smooth curve that approaches  $Q_{\text{ext}} = 2$ . The largest oscillations about this curve are those associated with nonabsorbing particles ( $m_i \sim 0$ ) and the amplitude of these oscillations decreases as the value of  $m_i$  increases, which is very clearly seen in the soot and dust like particles as compared to 75%  $\text{H}_2\text{SO}_4$  and oceanic particles. In oceanic and 75%  $\text{H}_2\text{SO}_4$  particle profiles the absorption curve exhibits several peaks and troughs, while in soot and dust like particles they are relatively smooth.

It is seen that  $Q_{\text{sca}} = Q_{\text{ext}}$  for nonabsorbing particles and with increasing particle size,  $Q_{\text{sca}}$  approaches 2, indicating that the scattering cross section is twice the geometric cross section of the particle. In this case, as we are in the realm of geometric optics, the problem can be discussed in the known terms of reflection, refraction and diffraction. It may seem at first surprising that  $Q_{\text{sca}}$  is 2 rather than unity. This is known as 'extinction paradox'. It is seen that, except for the infinitesimal fraction of the energy that propagates along the axis of the sphere, all of the geometrically intercepted radiation will undergo a change in direction because of reflection and/or refraction and thus half of the predicted magnitude of  $Q_{\text{sca}}$  can be explained. The other half arises from the radiation that is diffracted by the periphery of the sphere. The 'edge' of the sphere is identical to the edge of a hole of the same diameter in an opaque screen, as far as the diffraction effects go. This is known

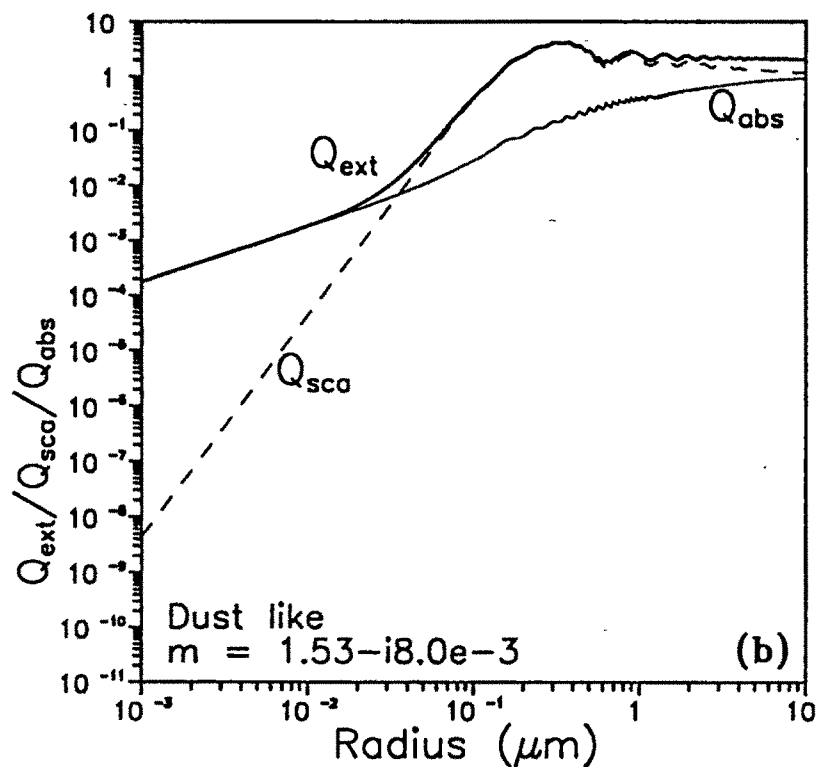
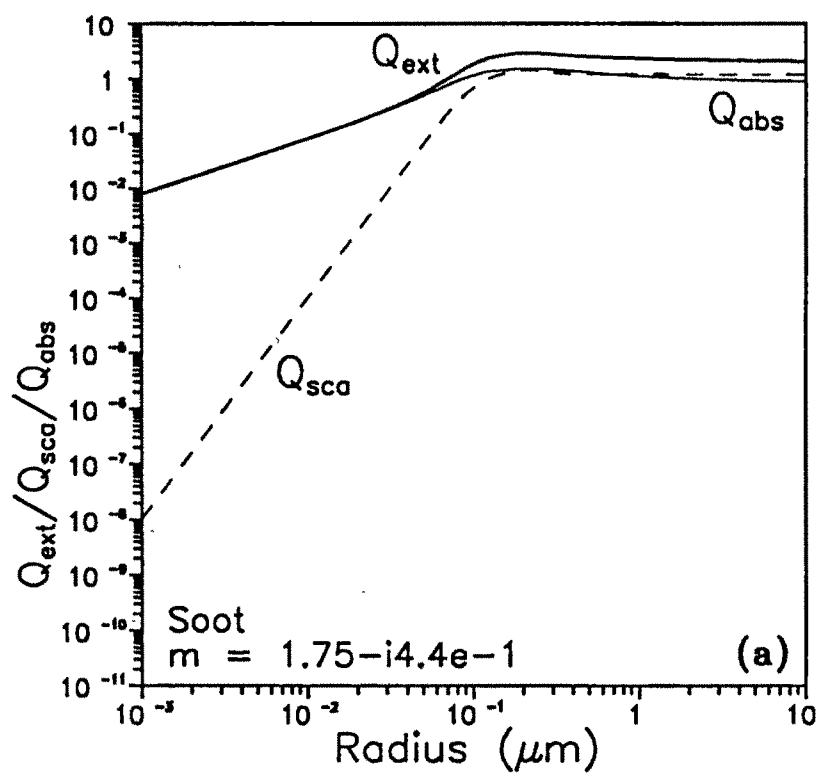
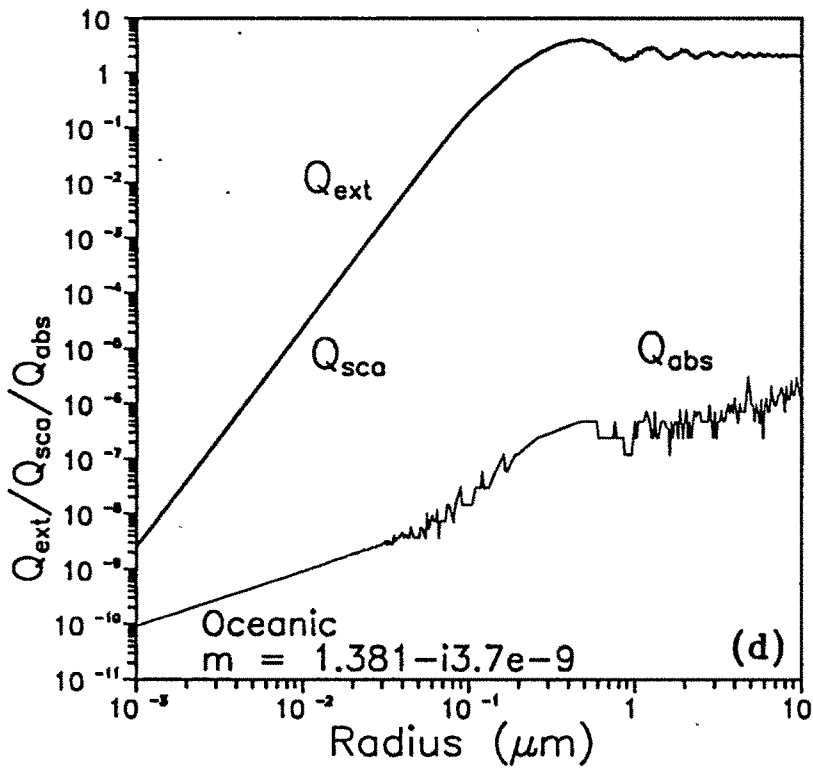
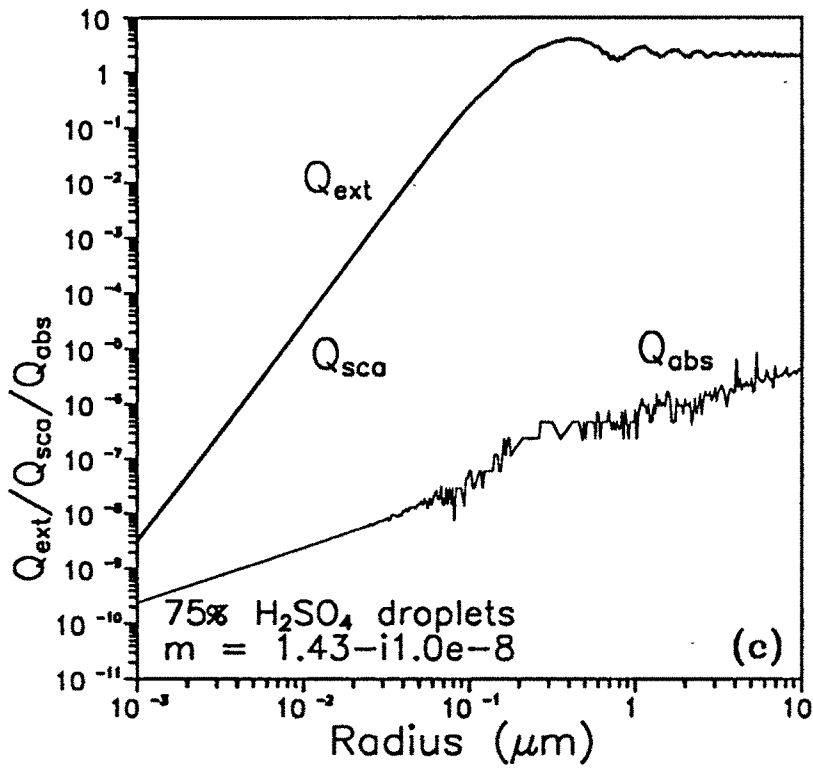


Figure 2.5: Extinction efficiency ( $Q_{ext}$ ), scattering efficiency ( $Q_{sca}$ ) and absorption efficiency ( $Q_{abs}$ ) at  $\lambda = 550 \text{ nm}$  for (a) soot (b) dust like (c) 75%  $\text{H}_2\text{SO}_4$  droplets and (d) oceanic aerosol particles.



as *Babinet's principle*. The diffraction pattern is the result of the interference of wave fronts from the edges and therefore it is not essential to know whether the outer edge of the disc is considered or the inner edge of the hole. The total scattered light comes from the light geometrically intercepted by the particle (reflected and refracted) plus from an equal amount of edge-diffracted light. Hence,  $Q_{sca} = 2$  for nonabsorbing particles in the larger size limit. But as  $m_i$  increases, the amount of light absorbed by the particle increases and the fraction of the intercepted light refracted by the particle gets decreased and in that case major contribution to  $Q_{sca}$  comes from the light diffracted by the edge and it therefore approaches unity in the large size limit for absorbing particles [Cadle and Grams, 1975].

#### 2.2.4 Angular distribution of the scattered light intensity of single particle

The angular distribution of the scattered intensity is described by the phase function. In case of Rayleigh scattering, no angular variation in the scattered radiation intensity is observed along the scattering plane perpendicular to the electric vector of an incident polarised light beam and a  $\cos^2\theta$  variation is observed in the parallel plane (Figure 2.6a).

The angular distribution of the scattered radiation intensities for aerosol particle of radius 0.01, 0.1, 1.0 and 10.0  $\mu\text{m}$  are plotted in Figures 2.6b-e, where  $i_{total}$  refers to the total intensity and is  $(\frac{i_{perpendicular} + i_{parallel}}{2})$ ,  $i_{perpendicular}$  refers to the intensity scattered in the perpendicular plane to the electric vector of the incident beam and  $i_{parallel}$  refers to the intensity in the parallel plane. These figures illustrate the effect of increasing particle size, from a smoothly varying function at 0.01  $\mu\text{m}$  to a highly distorted function with troughs and peaks at 10.0  $\mu\text{m}$ . Although these calculations have been done for  $\lambda = 550$  nm and for a dust like particle ( $m = 1.53 - i8 \times 10^{-3}$ ), the behaviour shown in the graphs is representative of the general behaviour of most of the commonly observed aerosols. It is evident that a larger portion of the energy is scattered in the forward direction as the particle size increases. It is also noticeable that a great deal of structures can exist in the angular distribution of the scattered radiation and the structures are prominent as the particle size increases. Practically, much of these strongly marked structures disappear when we consider the results of a polydispersed aerosol i.e. when applied to a size

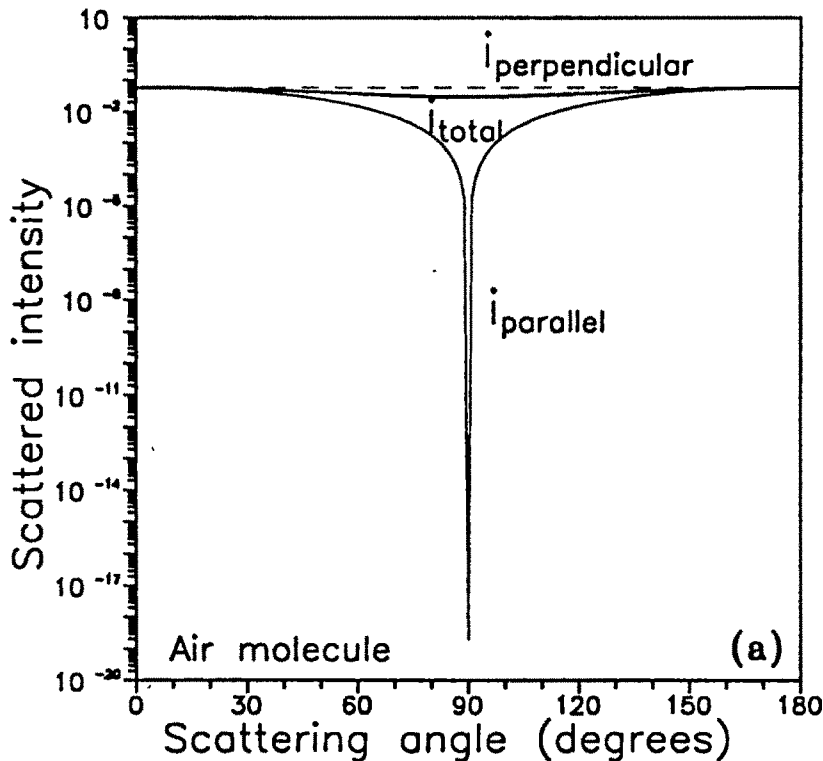


Figure 2.6: *The angular distribution of the scattered radiation intensity for an air molecule.*

distribution consisting particles of all sizes.

### 2.2.5 Mie scattering for many particles

$Q_{\text{ext}}$ ,  $Q_{\text{sca}}$  and  $Q_{\text{abs}}$  determined for individual particle using Mie theory when integrated over the entire particle range of an aerosol size distribution,  $\beta_{\text{ext}}$ ,  $\beta_{\text{sca}}$  and  $\beta_{\text{abs}}$  are obtained and the integration of the scattered intensities gives the aerosol phase function. Aerosol phase function essentially determines the fraction of intensity scattered at an angle. The aerosol phase functions calculated for 75%  $\text{H}_2\text{SO}_4$  droplets are shown in Figure 2.7 as examples. The phase functions for different size distributions are normalised at  $0^\circ$  scattering angle for comparison. In Junge size distributions (Figure 2.7a) the aerosol phase functions are smooth while in lognormal distributions (Figure 2.7b) the aerosol phase functions develop small disturbances when mode radius is  $1.0 \mu\text{m}$  while for all the

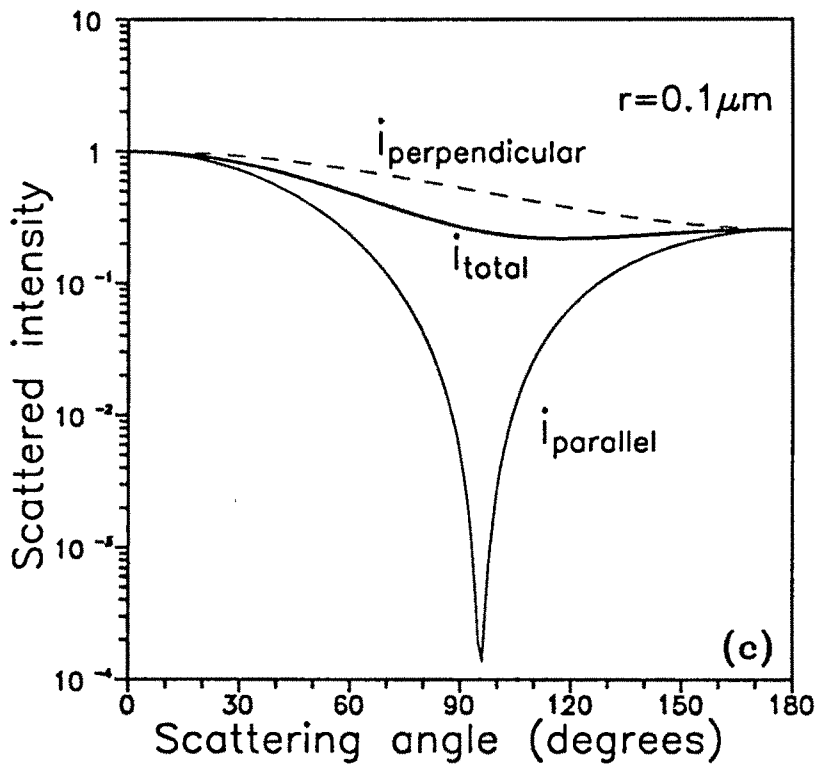
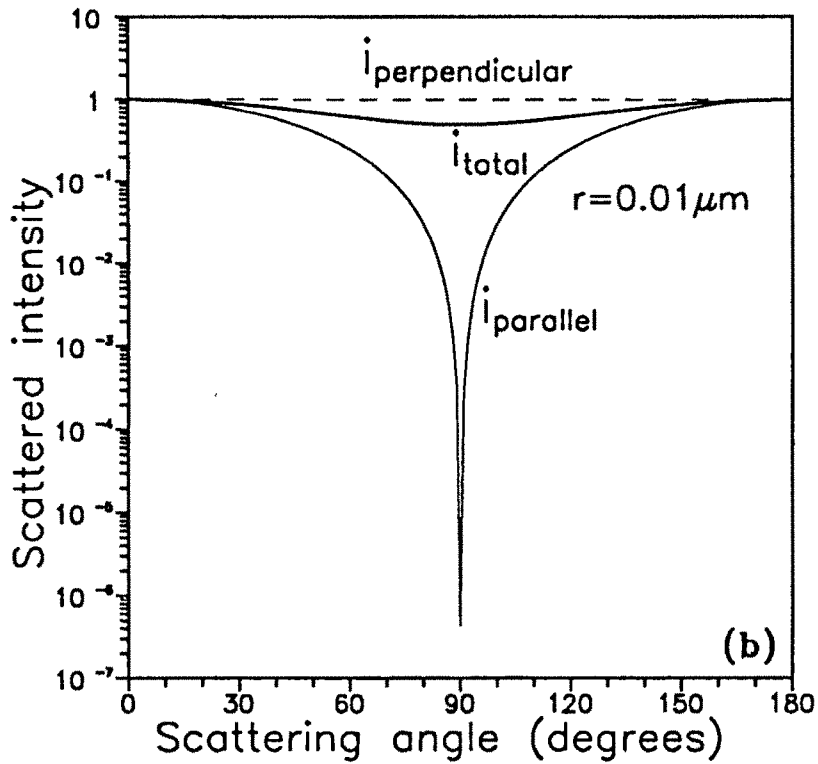
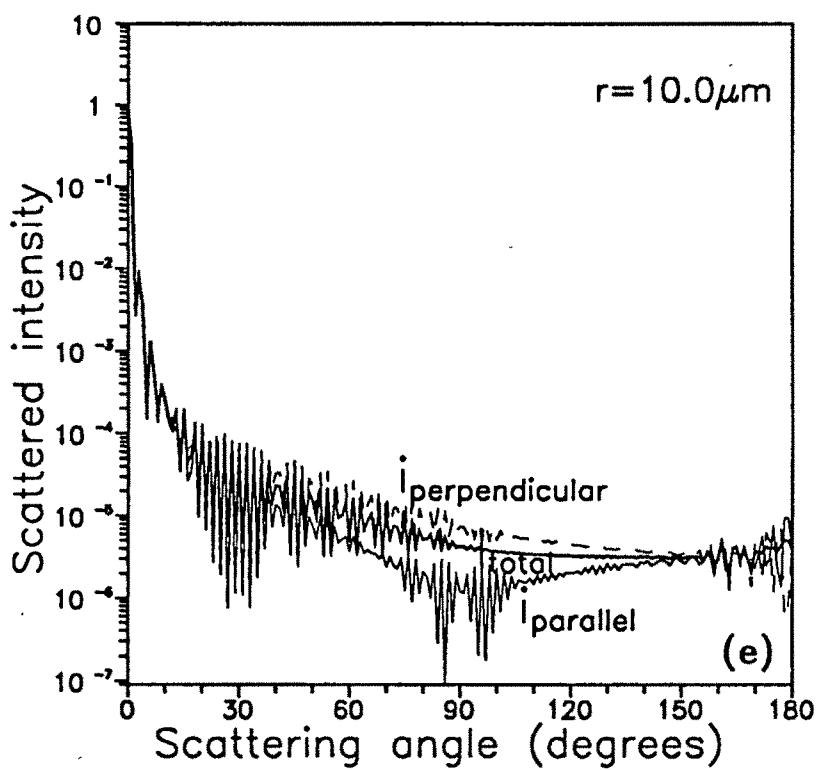
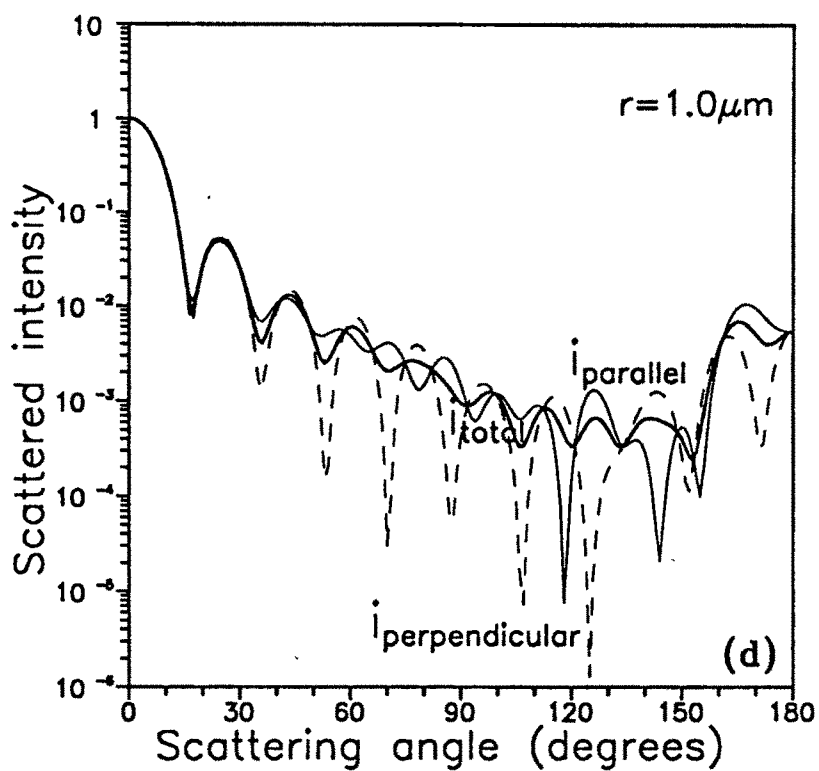


Figure 2.6: The angular distribution of the scattered radiation intensities for dust like aerosol particles of various sizes in both perpendicular and parallel directions and the total intensities.



mode radii ranging from  $0.07 \mu\text{m}$  to  $0.5 \mu\text{m}$ , the aerosol phase functions are smooth. This difference is mainly due to the assumed lower and upper radii limits used in the integration which are different.

Junge size distributions for various  $\nu$  values are calculated for  $r_{\min} = 0.04 \mu\text{m}$  and  $r_{\max} = 10.0 \mu\text{m}$  while in lognormal distributions  $r_{\min}$  and  $r_{\max}$  are chosen such that the aerosol number density falls by  $1 \times 10^{-6}$  with respect to the maximum value in the size distribution. Even in the case of Junge size distribution, for  $\nu = 2.0$ , the aerosol phase function shows some disturbances although they are not as marked as in the case of lognormal distribution, for  $r_m = 1.0 \mu\text{m}$ . So as the mode radius increases and  $\nu$  decreases the size distributions encompass more and more large particles and the cumulative phase function also develops some fluctuations due to structures in the individual scattered intensity distribution, as we have seen above. And also it is evident that as the number of large particles increases in a size distribution more and more radiation is scattered in the forward direction when compared to backward direction.

To investigate the dependence of aerosol phase functions on the type of particles i.e. on the refractive index, computations were done for four aerosol types exhibiting a wide range of refractive index values and for different  $\nu$  values. The results of computations are shown in Figure 2.8. For comparison the aerosol phase functions have been normalised at  $0^\circ$  scattering angle. Results indicate that the aerosol phase function depends more on size parameter than on different aerosol types. Though the results of Junge size distributions are shown as an example, the above fact is valid for lognormal distributions also. Also the phase functions for  $\nu = 2.0$  and  $4.0$  are shown for various models and for the sake of clarity, for  $\nu = 3.0$ , only the dust like particle's phase function is shown.

Aerosol phase functions obtained for  $g$  values varying from  $0.6$  to  $0.9$  at  $550 \text{ nm}$  are plotted in Figure 2.9. As asymmetry factor is an average of the cosine of the scattering angles, the disturbances in the phase functions derived using  $\nu$  are not present in these curves and a smooth picture is obtained. With decreasing  $\nu$ , the relative number of larger particles increases, which results in an increase in  $g$  as can be seen in Figure 2.9.

Mie scattering theory assumes that scattering particles in the atmosphere are homogeneous spheres. But in reality particles can have aspherical shapes such as ellipsoid, spheroids, oblate etc. and so the implications of the assumption of all the scattering

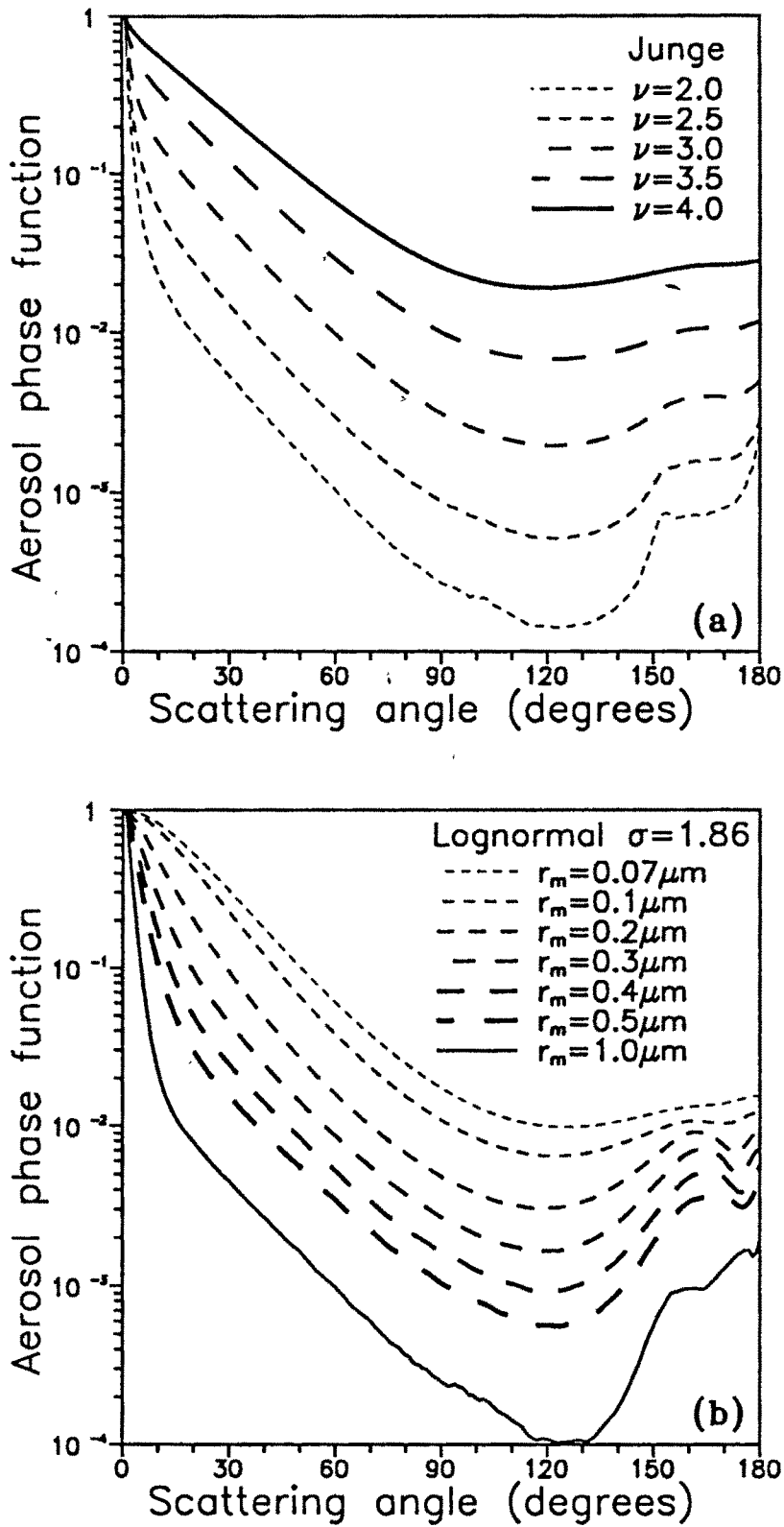


Figure 2.7: Aerosol phase functions  $P_a(\lambda, \theta)$  for (a) Junge size distributions having exponents from 2 to 4 in steps of 0.5 for an ensemble of particles from  $0.04\mu\text{m}$  to  $10.0\mu\text{m}$  and (b) lognormal distributions for various mode radii from  $0.07\mu\text{m}$  to  $1.0\mu\text{m}$ .

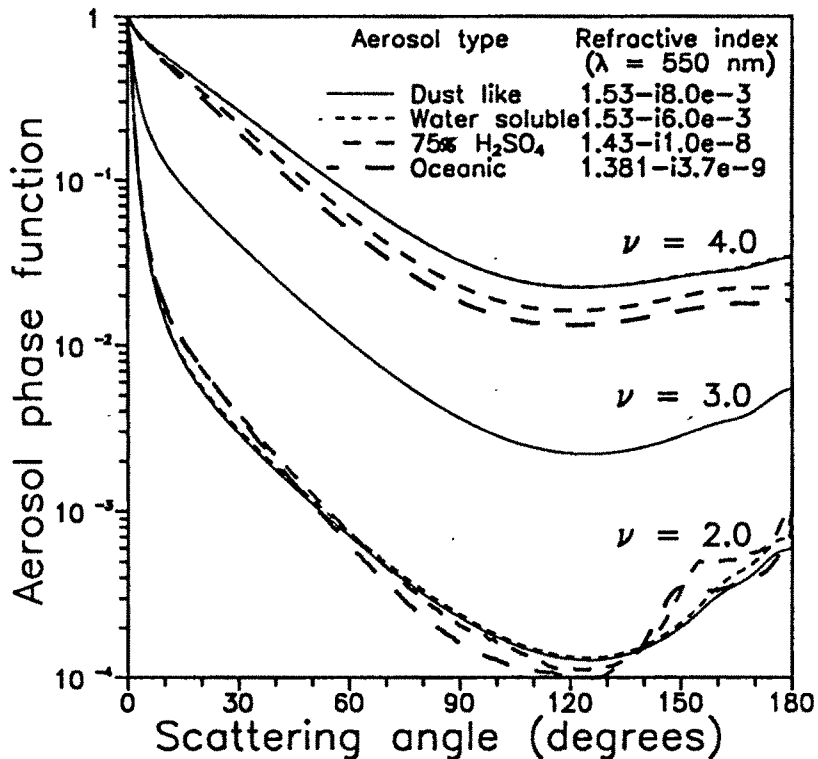


Figure 2.8: Aerosol phase functions for various aerosol types for  $\nu = 2, 3$  and  $4$ . The curve shows the dependence of aerosol phase function more on  $\nu$  than on various aerosol types.

particles to be spheres needs investigation. *Holland and Gagne* [1970] used a polar nephelometer to study scattering from irregularly shaped particles with an emphasis on the differences between the measured scattering parameters and those calculated from Mie solution for homogeneous spheres. In the forward direction (i.e. for angles  $< 90^\circ$ ) a good agreement was found but in the backward scattering (i.e. for scattering angles  $> 90^\circ$ ) the scattered intensity was found to be less than that predicted for spherical particles. Recently *Koepke and Hess* [1988] found that the scattering functions of nonspherical particles compared with those of equivalent spheres show differences with increasing particle size. They also found that for aerosol types with a relatively low amount of large particles such as continental and urban aerosols, the effect due to uncertainty about particle shape can be ignored. For desert aerosols, which are larger in size an appreciable difference in

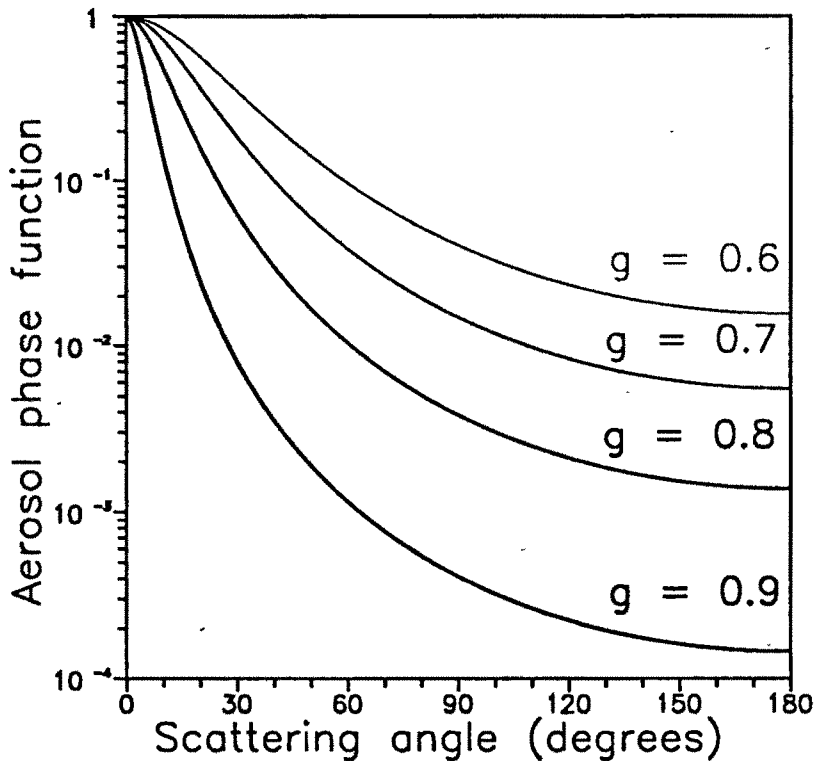


Figure 2.9: Aerosol phase functions obtained for asymmetry parameter  $g$  varying from 0.6 to 0.9.  $g$  is defined as the average of the cosine of the scattering angles for scattered radiation.

the scattering functions was found beyond 120°. However, as in the present work aerosol scattering phase functions have been compared only between 0° and 90° the question of effect of nonsphericity on the derived aerosol parameters does not arise.

Using LOWTRAN 7 code multiple scattering calculations were performed for solar zenith angles varying from 0° to 80° from 300 to 1000 nm for a model atmosphere which was made up of Urban (0-2 km), Tropospheric (2-10 km), High/Aged volcanic (10-30 km) and Meteoric dust (30-100 km) aerosol models. The results indicate that multiple scattering is important only at low altitudes between 0 and 4 km for 300 nm and at 500 nm. However, above about 5 km the influence of multiple scattering on the scattered radiation is almost nil. The irradiance at any point in the atmosphere is a combination of direct solar radiation and radiation scattered more than once. Thus the inclusion of multiple

scattering will only enhance the estimated radiation values. However, this increase in intensity to the direct radiation is negligibly small. In the balloon-borne measurements as the observations are done above 5 km and in ground based Sun photometry measurements as only the total loss of radiation in the medium is only measured i.e. optical depth, the effect of multiple scattering is neglected, in the present work.

## 2.2.6 Size range of aerosols for optical investigations

In a size distribution there is a tendency for number of particles to increase rapidly with decreasing particle size, making small particles the most important ones as they are numerous, while studying the optical effects. Though in a given volume of aerosol, the number of larger particles is orders of magnitude less when compared to smaller particles, as the cross section increases with the square of radius, the large particles can still dominate aerosol optical effects because their cross section per particle is significantly larger than that of smaller particles. The shape of the size distribution function (i.e. the relative number concentrations of large and small particles) obviously is important for establishing the size ranges that must be measured to draw any conclusion concerning the optical properties of aerosols.

To determine the size range of aerosols suitable for optical investigations, Junge size distribution ( $\nu = 3$ ) and lognormal distribution function ( $r_m = 0.3 \mu\text{m}$ ,  $\sigma = 1.86$ ) for 75%  $\text{H}_2\text{SO}_4$  droplets ( $1.43 - 11.0 \times 10^{-8}$ ) and dust like particle ( $1.53 - 18.0 \times 10^{-3}$ ) at  $\lambda = 550 \text{ nm}$  are considered. The lower ( $r_1$ ) and upper radii ( $r_2$ ) limits are set as  $0.01 \mu\text{m}$  and  $10.0 \mu\text{m}$  in the calculations of  $\beta_{\text{ext}}$ ,  $\beta_{\text{sca}}$  and  $\beta_{\text{abs}}$  and these quantities were calculated as a function of  $r_1$  varying from  $0.01 \mu\text{m}$  to  $10.0 \mu\text{m}$  for both the size distributions and for both aerosol types. The results obtained were normalised by dividing all the intermediate values of  $\beta_{\text{ext}}$ ,  $\beta_{\text{sca}}$  and  $\beta_{\text{abs}}$ , by the values obtained for the  $r_1 = 0.01 \mu\text{m}$ ,  $r_2 = 10.0 \mu\text{m}$  case. The results of  $\beta_{\text{ext}}$  are shown in Figure 2.10.

For both the size distributions it is seen that the major contribution to  $\beta_{\text{ext}}$  occurs in the size range from  $0.1$  to  $2.0$ - $3.0 \mu\text{m}$  radius. The same is true for  $\beta_{\text{sca}}$  and  $\beta_{\text{abs}}$  also and hence are not plotted. So depending on the experimental technique employed and the parameter of interest, say  $\nu$  in Junge size distribution and  $r_m$  and  $\sigma$  in LND, both the size distributions can adequately be used, provided they cover the important aerosol range

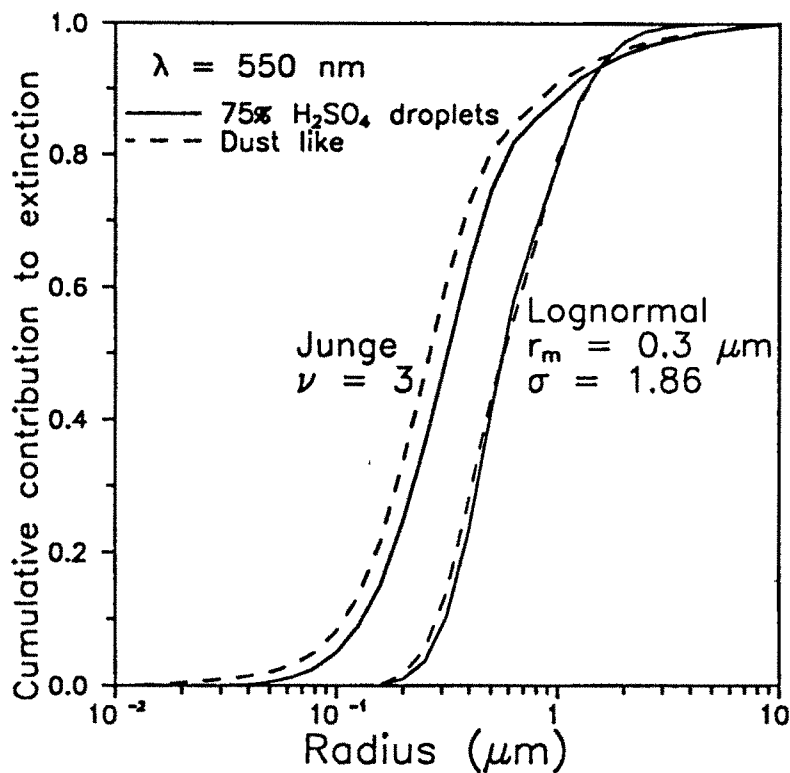


Figure 2.10: Cumulative contribution of  $Q_{ext}$  to  $\beta_{ext}$  by particles of sizes from 0.01 to 10.0  $\mu m$  for Junge and lognormal size distributions for 75%  $H_2SO_4$  droplets and dust like particles.

of 0.1-3.0  $\mu m$ . Though in general, this is the range suitable for optical investigations, observations have shown that desert and sea salt aerosols can have radius of 20  $\mu m$  and above, but the number density of these aerosols is small and also their residence times are very short [d'Almeida *et al.*, 1991]. It is not ascertained how long particles above 20  $\mu m$  can remain in the atmosphere in an urban environment and whether can take part in the radiative transfer process.

## 2.2.7 Spectral dependence of aerosol extinction coefficients and its dependence on relative humidity

The spectral (wavelength) exponent  $\alpha$  defined by Ångström as

$$\beta_{\text{ext}} = k \lambda^{-\alpha} \quad (2.15)$$

where  $k$  is Ångström coefficient can be obtained by plotting the aerosol extinction coefficients with respect to wavelength on a log-log scale wherein the slope of the curve determines  $\alpha$ . In this section an attempt is made to determine  $\alpha$  for various aerosol types and models in the visible wavelength and near infrared ranges and the results are discussed.

The aerosol extinction coefficients are calculated for various models and aerosol types obeying lognormal distributions given by *d'Almeida et al.* [1991] for the wavelength region 300 to 1050 nm and  $\alpha$  is determined.

In Figure 2.11  $\beta_{\text{ext}}$  obtained for a 75%  $\text{H}_2\text{SO}_4$  particle for different mode radii are plotted. It is apparent that the extinction coefficients increase for a size distribution when the mode radius is large whereas they decrease for a small mode radius. This in general is valid for all types of particles.  $\alpha$  varies from 1.5 for 0.07  $\mu\text{m}$  to about  $-0.1$  for 1.0  $\mu\text{m}$ , which clearly shows that as the mode radius increases, keeping the width of the size distribution constant, it encompasses more and more large particles, which leads to a lower  $\alpha$  value and also the extinction coefficient shows almost a linear dependence with respect to wavelength. The same result is found to be true for various widths of the size distribution, keeping the mode radius  $r_m$  constant. So in general, it becomes essential to know two different quantities in order to adequately describe aerosol extinction in the atmosphere. They are refractive index of the particle, especially the imaginary part of it, as it conveys the absorption characteristics of the particle and particle size distribution. Apart from these two, it is essential to know the particle shapes, which we assume to be spherical.

The permanent presence of water vapour in the atmosphere, except in the arid and semiarid regions, affects the aerosol by aiding it to grow bigger or shrink in size. The growth of aerosol particle results in a change in the size, shape and chemical composition of the particle and affects the radiative characteristics owing to changes in the radius and

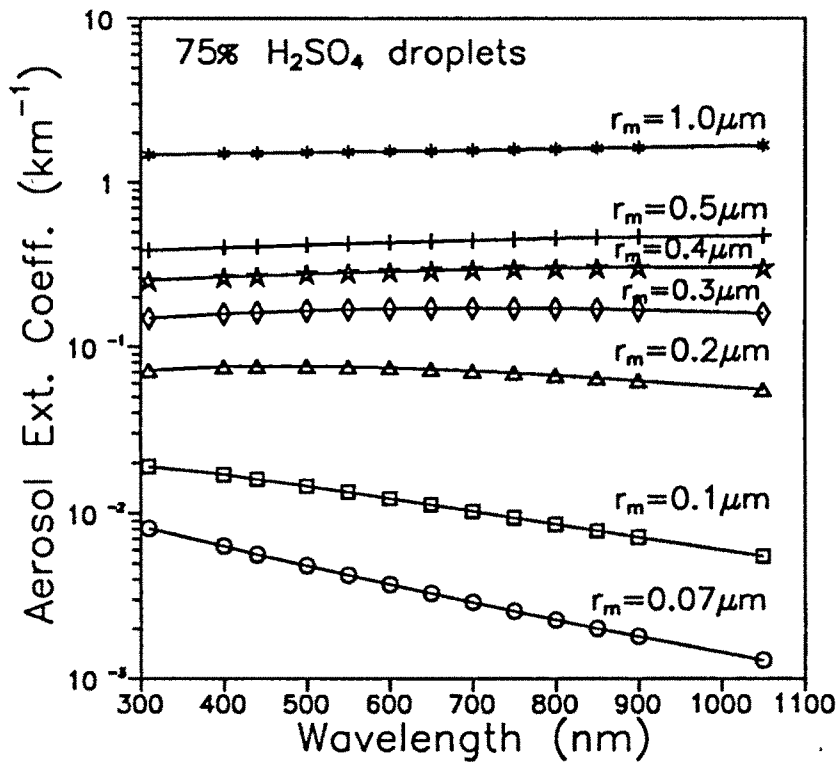


Figure 2.11: *Aerosol extinction coefficients for a lognormal size distribution having mode radius varying from 0.07 to 1.0  $\mu\text{m}$  show that as the mode radius increases the size distribution encompasses more and more larger particles and the dependence of extinction on the particle size becomes less.*

refractive index [Hänel, 1976].

The aerosol extinction coefficients from 300 to 1000 nm for various relative humidity classes ranging from 0% to 99% given by *d'Almeida et al.* [1991] have been used to determine  $\alpha$ . The aerosol extinction coefficients are found to increase in general with increasing relative humidity, but in a distinct way, representative of the various components present in the model. But  $\alpha$  values give interesting results. In Figure 2.12 the variation of  $\alpha$  with relative humidity is plotted for six aerosol models.

For Polluted maritime, Clean continental, Average continental and Urban aerosol models, the  $\alpha$  values decrease with increasing relative humidity and the effect is more prominent when the relative humidity is higher than 80%. Interestingly Clean maritime

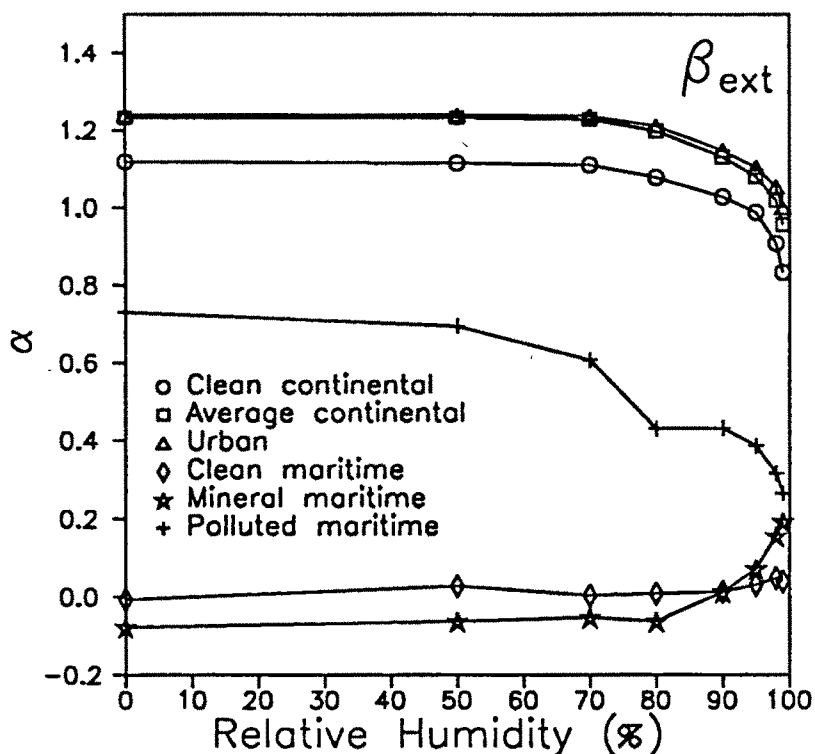


Figure 2.12: The variation of Ångström's wavelength exponent  $\alpha$  with respect to change in relative humidity for six aerosol models.

shows almost no change in  $\alpha$  value with increasing relative humidity. Mineral maritime model which consists of larger particles has a  $-\alpha$  value at 0% relative humidity and then approaches toward  $+\alpha$  as the relative humidity increases.

Single scattering albedo ( $\omega_0$ ) is a parameter which has application in climate modeling studies and in satellite inversions while using the radiative transfer code. Essentially single scattering albedo determines whether the Earth-atmosphere system gets cooler or warmer because of the presence of aerosols. Weakly absorbing aerosols ( $\omega_0 \sim 1$ ) which predominantly scatter radiation, increase the amount of energy backscattered to space. As the energy input to the Earth-atmosphere system gets reduced, it results in a net cooling of the system. The magnitude of this increase in planetary albedo is a function of particle size, optical depth and the location of the aerosol layer [Ackerman, 1988]. The asymmetry factor  $g$  at a given wavelength increases with increasing particle size for a

fixed aerosol composition, thus the smaller particles tend to increase the planetary albedo in comparison to large particles for the same optical depth. Absorbing aerosols ( $\omega_0 \leq 0.8$ ) tend to reduce the solar energy lost from the Earth-atmosphere system by absorbing solar radiation that otherwise would be reflected from clouds and from the surface. The Earth-atmosphere system would then get warmed up as the energy input gets increased. But after large volcanic eruptions, large amount of sulphate particles are present in the stratosphere. Though  $\omega_0$  is nearly 1 for these particles in the visible wavelength range, in the infrared region they are highly absorbing, leading to a heating due to the absorption of solar radiation as well as the upwelling thermal radiation. This effect is seen where the aerosol layer is present and as the layer scatters the incoming solar radiation a cooling effect will occur in troposphere, as was seen after El Chichon and Mt. Pinatubo eruptions. *Pollack et al.* [1981] estimated that when  $\omega_0$  becomes  $\leq 0.98$  it would change the sign of climate forcing from cooling to heating. Various aerosol types can have  $\omega_0$  varying from 0.1 to about 0.9 depending on wavelength and season [*d'Almeida et al.*, 1991].